applied sciences

MDPI

Article

Influence of Steel Section Configuration on the Seismic Performance of Concrete-Encased Steel Rectangular Bridge Piers

Mohammadreza Moradian and Munzer Hassan *

Department of Construction Engineering, École de Technologie Supérieure, University of Quebec, Montreal, QC H3C 1K3, Canada; mohammadreza.moradian.1@ens.etsmtl.ca
* Correspondence: munzer.hassan@etsmtl.ca

Featured Application

Optimized concrete-encased steel (CES) bridge piers offer a high-ductility, energy-dissipative solution for seismic-resistant bridge design in Canadian conditions.

Abstract

Concrete-encased steel (CES) bridge piers can be considered as a robust alternative to traditional reinforced concrete sections, especially in regions prone to seismic activity. CES piers combine the ductility of steel with the compressive strength of concrete, offering improved energy dissipation and resilience during earthquakes. Given the lack of CES design specifications in the Canadian design code, it is crucial to compile a body of knowledge describing the behavior of the CES bridge pier in order to facilitate the codification of the design guide. This study assesses the seismic performance of CES rectangular bridge piers with a focus on how variations in the steel section configuration affect the pier's overall behavior under seismic loads. To conduct this assessment, a fiber element model was employed to model CES bridge piers subjected to seismic loading. The thickness and height of the web and the width and the thickness of the flanges of the I-shape steel section were varied to understand their impact on the bridge's seismic performance. In addition to the I-shape sections, a crossed two-I-shape section was also studied. Spectral analysis, nonlinear pushover analysis and nonlinear time-history analysis was performed on the bridge models in order to better understand the seismic performance of the studied bridge piers. Simulation results indicate that larger flanges increase the pier's bending moment capacity, allowing it to absorb greater seismic energy and undergo larger deformations without failing. This increases the overall ductility of the pier and enhances its ability to dissipate seismic energy. However, excessively large flanges or web can reduce the concrete cover and reduce the durability of the pier in the context of Canadian extreme-winter conditions. The study concludes that a balance between web thickness and flange width must be achieved to ensure the bridge can resist seismic forces while maintaining sufficient ductility and energy dissipation. Therefore, an optimized design, according to seismic demands, enhances the overall resistance of CES bridge piers.

Keywords: bridge pier; concrete-encased steel (CES); performance-based design; plastic hinge; highly confined concrete; partially confined concrete; time-history analysis; pushover analysis

Academic Editors: Valentino Paolo Berardi and Maria Favvata

Received: 25 January 2026
Revised: 7 March 2026
Accepted: 11 March 2026
Published: 16 March 2026

1. Introduction

The use of concrete-encased steel (CES) columns for bridges has lots of advantages as they offer some unique characteristics such as durability and seismic resistance while being resistant to harsh environmental factors. Equally, they have their pros and cons, such as other factors that need to be considered when using these columns.

One of the primary advantages of concrete-encased steel columns is their enhanced durability. In areas that have rough winters, roadway de-icing chemicals are used, which can lead to rapid deterioration of exposed steel. Steel is put under a lot of stress and is highly prone to corrosion or rust, which is aggravated in cold climates with moisture and de-icing salts [1]. The encasement in concrete provides a protective layer that shields the steel from direct exposure to dew and salt, thereby lowering the risk of corrosion and increasing the lifespan of the bridge. Figure 1 presents a typical concrete-encased steel section.

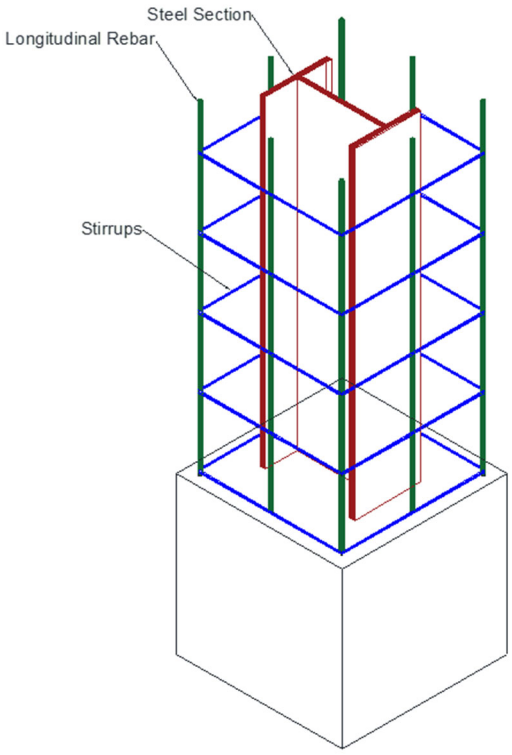

Figure 1. Configuration of the concrete pier for concrete-encased steel (CES) section.

The method of composite construction has been utilized across the globe since the 1930s for gravity and lateral load-bearing structures of buildings and bridges. All over the world, there is a large range of structures, mostly buildings, that have outdated and inadequate concrete-encased steel (CES) columns. These are steel columns encased in concrete constructed prior to the implementation of seismic design details in the 1980s. More of these intermediate CES columns using concrete-encased steel are preferred in high-seismic regions. The need for non-prescriptive or performance-based design of tall buildings and bridges has increased as a result of the significant increases in building and bridge numbers, heights, and architectural irregularities in the modern construction industry. This has led to many buildings and bridges exceeding the irregularity limits of design codes. Modern tall structures in seismically active regions of the world, particularly the United States, are increasingly using CES columns. However, the application of CES sections in bridges has not increased yet. Since the 1970s, CES articles have become less popular in the United States.

However, some research work on the structural behavior of CES columns can be found. One analytical study showed how the steel core affects the confinement of concrete in CES short columns [2]. The authors proposed confinement factors for rectangular sections with different steel shapes and reinforcement layouts. These factors work well for rectangular sections with ties but not for circular ones with spirals. Later, Ellobody and Young [3] studied CES columns under axial load with a 3D finite element model using these factors, and then they also analyzed columns with eccentric loading.

Another study reviewed rectangular CES columns using different design codes, including ACI 318, AISC-LRFD and the AISC Seismic Provisions [4]. Both referenced papers used fiber section analysis to examine the nonlinear behavior of steel and concrete and suggested that the criteria for design limits should be re-evaluated.

Further experimental research was performed on CES columns in the laboratory under monotonic and cyclic loading to study their behavior and failure modes [5]. Some researchers have also studied the use of high-strength concrete in CES columns. For example, Lai et al. [6] carried out experimental and numerical analyses on the buckling behavior of steel columns encased with high-strength concrete.

One of the most relevant experimental and analytical studies on the behavior of CES bridge columns was performed by Naito et al. [7]. Their work focused on the ductility of different rectangular sections, and they proposed a modification to an equation in [8] to better estimate the plastic hinge length of CES columns.

Recent studies have continued to investigate the seismic and axial–flexural behavior of concrete-encased steel composite columns. Experimental work reported in [9] examined the cyclic performance of steel-reinforced composite concrete columns under combined axial and lateral loading, showing the importance of confinement and steel contribution in improving ductility and strength. Numerical parametric analyses presented in [10] demonstrated that fiber-based modeling approaches can accurately capture the axial force–bending moment interaction behavior of composite beam–columns and allow efficient evaluation of different cross-section configurations. More recently, experimental investigations on high-strength CES columns reported in [11] confirmed that improved material strength and confinement significantly enhance energy dissipation capacity and post-yield stability. These recent findings highlight the growing interest in CES structural systems and support the need for additional parametric studies focused on optimizing cross-section configurations for seismic performance.

There are worries over how well CES columns can withstand severe seismic events. During an earthquake, non-ductile concrete features were found to be the source of damage and collapse [12]. The seismic behavior of CES composite columns in bridges is highly understudied, according to the literature. Important unknowns for these CES columns include strength, ductility, drift capacity, cyclic backbone curves for nonlinear performance-based seismic assessment, residual axial capacity, numerical criteria to differentiate seismic modes of failure, and seismic acceptance criteria. In order to investigate the seismic capacity of CES bridge piers with rectangular columns, three CES columns were analyzed under seismic loading. The seismic demand, nonlinear behavior and failure mechanism were investigated and analyzed.

The most recent studies have continued to investigate the structural behavior and seismic performance of concrete-encased steel (CES) and steel-reinforced concrete (SRC) composite members through both experimental and numerical approaches. For example, Shang et al. [13] studied the lateral load–displacement response of flexure-dominant CES columns and showed that the interaction between the encased steel section and surrounding concrete significantly improves the strength, stiffness, and deformation capacity of the column under seismic loading. In addition, Idriss and Gamal [14] proposed an adaptive

neuro-fuzzy prediction model to estimate the structural behavior of CES columns under axial and uniaxial loading conditions, demonstrating the growing interest in advanced analytical and computational approaches to evaluate CES structural performance. Experimental investigations on composite structural systems were also conducted by Wang et al. [15], who studied the seismic behavior of SRC column–RC slab joints through cyclic loading tests and numerical analysis, showing that composite steel–concrete members can provide improved energy dissipation capacity and stable hysteretic behavior under seismic actions. These studies confirm the advantages of CES and SRC systems for structural applications in seismic regions. A more extensive literature review covering recent developments in the seismic evaluation of CES columns can be found in [16].

2. Analytical Study

To assess the seismic performance of CES bridge pier sections, a bridge model was developed and designed in accordance with the Canadian Highway Bridge Design Code (CHBDC) [17] requirements. Additionally, three different configurations of the steel profile section were considered to analyze and determine the most efficient configuration for the steel profile. The three studied sections have the same overall geometry, stiffness and resistance, and the dimensions and details are shown in Figure 2. The sections were designed to represent the structural column of a regular and commonly used road bridge in Canada. The selection of the steel profile section configuration was based on the literature review and previous studies on CES columns [16,18].

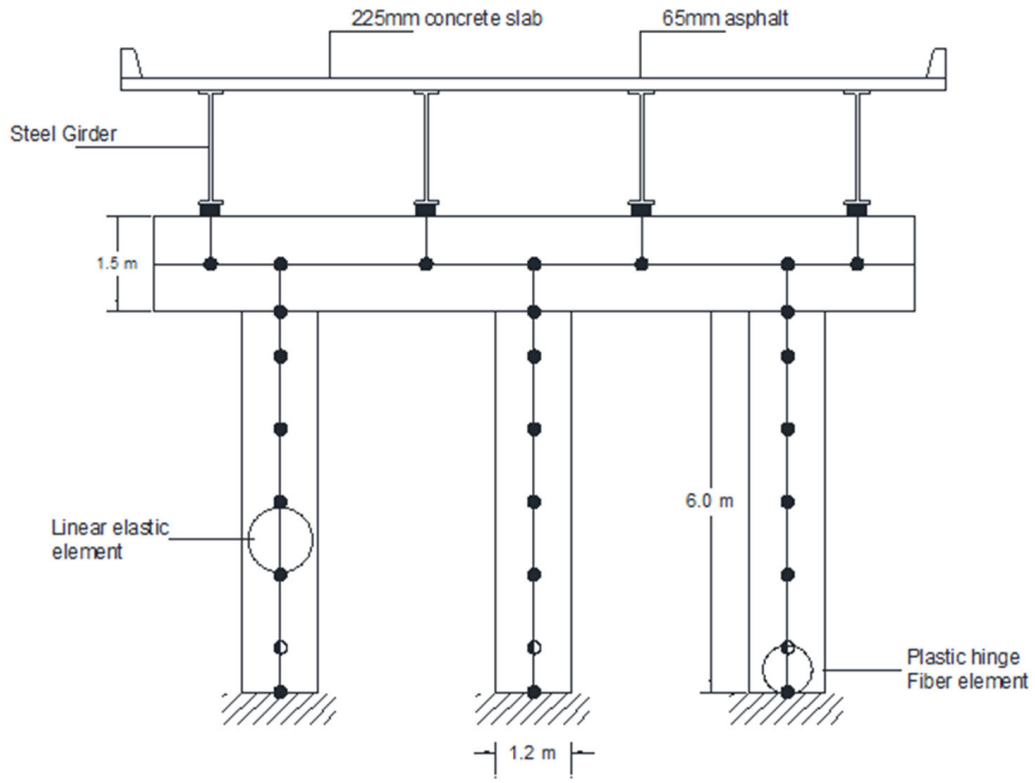

Figure 2. Elevation view of the bridge pier.

A typical slab-on-girder concrete bridge was considered in this study, representing many bridge structures found on North American highways. The bridge model has a total length of 80 m and an overall width of 13 m. It consists of two equal-span continuous straight spans, with the superstructure supported by two abutments and a central bend with three columns. The columns have a rectangular cross-section of 1200 mm × 1200 mm and a height of 6 m, as shown in Figure 2. The superstructure is made up of a 225 mm thick

cast-in-place concrete slab supported by four steel girders. At the abutments, the girders rest on roller bearings. The bearings on the central pier are restricted in longitudinal and transversal directions but they are free to rotate. The bridge is assumed to be founded on a soft-rock or very dense-soil site, corresponding to a class C site according to the CHBDC [17] soil classification. The concrete is specified to have a strength f'c of 35 MPa and a modulus of elasticity Ec of 28,165 MPa. For the steel reinforcement, a yield stress of fy = 400 MPa and a modulus of elasticity Es = 200,000 MPa were assumed.

A 3D model of the bridge was created using the CSiBridge-v26 software [19]. The bridge columns were modeled using nonlinear beam–column elements with fiber discretization of the cross-section along the plastic hinge length at both the top and bottom of the columns. In contrast, elastic beam–column elements were used in the regions outside the plastic hinges, as shown in Figure 2. The numerical model was developed using a three-dimensional nonlinear beam–column formulation with distributed plasticity. Each column cross-section was divided into concrete, rebars and structural steel fibers, enabling explicit consideration of nonlinear material behavior and interaction between steel and concrete components. Abutments were modeled with roller supports, free to move in the longitudinal direction and restrained in the transversal direction, and the central pier bearings were restrained in both longitudinal and transverse directions. All bearings are free to rotate. Material nonlinearities were introduced through constitutive relationships for highly confined, partially confined and unconfined concrete as well as nonlinear models for reinforcement and structural steel components.

The length of the plastic hinge was estimated using (Equation (1)). Based on the lateral displacement capacity of the column and its integration with the curvature distribution, Naito et al. [7] calculated and proposed Equation (1) for the length of the plastic hinge of the CES column.

$$L_{rp} = (0.5d + 0.05h)\left\{(1 + 0.04t_{ek})\frac{M_m}{M_{y0}} - 0.25\right\} + 12(D_r - 12) \quad (1)$$

In Equation (1), M_m is the maximal moment, M_{y0} is the yield moment, D_r is equal to the rebar diameter in mm, and t_{ek} is the ratio of A_s/A_r, where A_s is defined as the gross area of the steel section and A_r is the gross area of the longitudinal rebars. Also, d is considered as effective column depth, and h is the column length.

The longitudinal reinforcement for the CES bridge pier models was designed in accordance with the CHBDC [17] specifications for a lifeline bridge. The seismic design forces were derived from the results of multi-modal spectral analysis, where, to account for the cracked section, the column's effective inertia was set to 70% of its gross inertia (Ie = 0.7Ig) for the CES section, based on the equations recommended in CSA A23.3-14 [20]. Modal responses were combined using the complete quadratic combination (CQC) method, and the 30% rule was applied to combine the maximum responses obtained from separate analyses in the two principal directions of the bridge.

Dead load forces were combined with seismic design forces to determine the required longitudinal reinforcement steel ratios for the columns. For dead load, ratios of 1.25 and 0.8 were considered, in accordance with the load combination requirements of the CHBDC [17].

The transverse reinforcement for confinement in the plastic hinge regions of the columns consists of 20 M rebars spaced 75 mm center to center. Due to the lack of specific guidance for CES columns in the CHBDC [17], the requirements of CSA-S16 [21] were followed for both the longitudinal and transverse reinforcement of the CES section. The total longitudinal reinforcement area must exceed 4% of the gross cross-sectional area, and the concrete strength should range between 20 and 55 MPa. Additionally, the yield stress of the structural steel is limited to 350 MPa, while the yield stress of the reinforcement bars

should not exceed 400 MPa. It should be noted that due to the lack of requirements in the CHBDC [17] for the reinforcement of the CES section, the requirement of the CSA-S16 was met in order to assess the seismic performance of the CES section. Figure 3 presents a diagram showing the employed process of the analytical study.

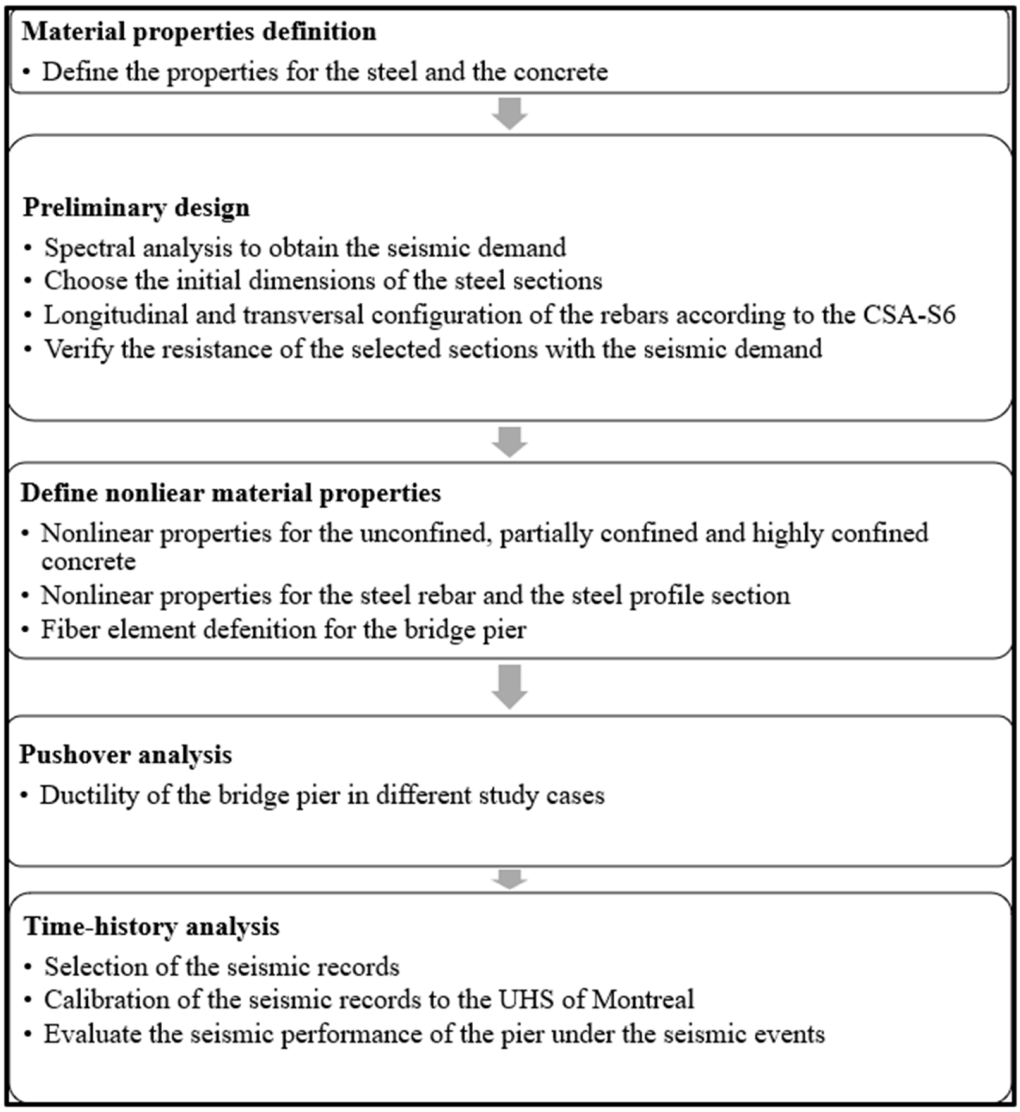

Figure 3. Process of the analytical study.

The cross-sectional design of the columns was carried out to meet the seismic load requirements specified by the CHBDC [17]. The 30% rule was applied to account for seismic loads in the two horizontal directions of the bridge. It is important to note that the R factor was set to 1.0 to assume an elastic behavior of the bridge during the preliminary design phase.

As a result, the longitudinal reinforcement for the three CES bridge piers was designed as shown in Figure 4. To assess the seismic behavior of the most optimal configuration for the CES bridge pier, a comparison between the three studied sections was conducted. The section CES 1 has a wide-flange steel section, the section CES 2 has a W-shape steel section and the section CES 3 has two crossed W-shape sections. All the models meet the seismic design requirement according to the CHBDC [17]. Table 1 presents the longitudinal steel ratio of each selected model.

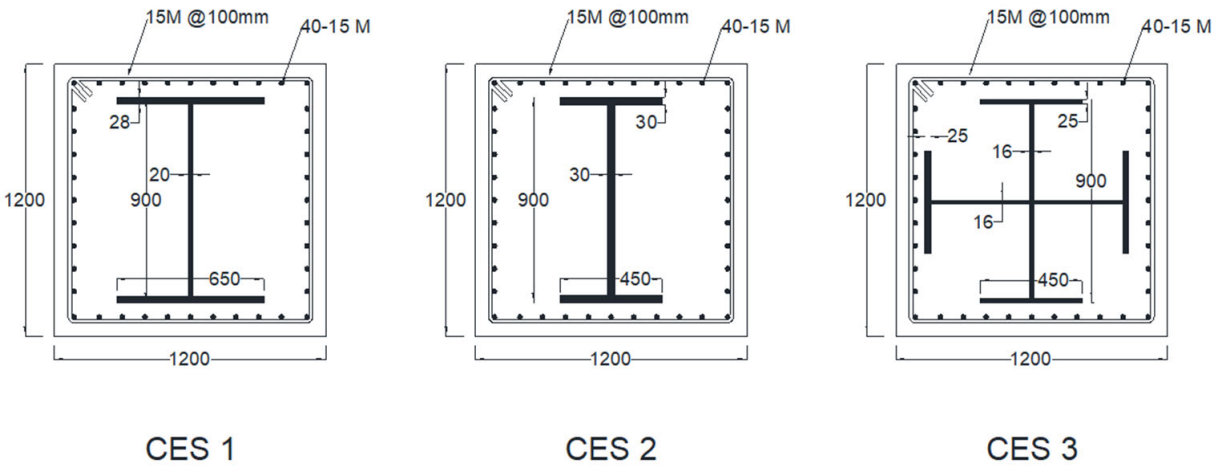

Figure 4. Reinforcement configuration of the studied columns.

Table 1. Reinforcement of the studied CES bridge piers.

Model	Fundamental Period (s)	Longitudinal Rebar	Steel Section Area (mm^2)	Longitudinal Rebar Ratio (%)	Steel Section Ratio (%)	Total Steel Ratio (%)
CES 1	0.731	8000	54,400	0.55	3.78	4.33
CES 2	0.747	8000	52,200	0.55	3.62	4.17
CES 3	0.765	8000	72,200	0.55	5.01	5.56

It should be noted that the capacity of the designed sections is considered 80% of the seismic demand according to the linear spectral analysis in order to optimize the steel section during the seismic performance analysis and compare the nonlinear analysis of the studied sections.

It should be emphasized that, to effectively compare the seismic behavior of the three studied bridge piers and determine the most optimal configuration of the steel section, the longitudinal rebar ratio was maintained as equal for all three bridge models. By doing so, the analysis isolates the influence of the different configurations of the steel core and other design factors, ensuring that any variations in performance can be directly linked to the changes in the steel section's design, rather than disparities in reinforcement ratio. This approach allows for a more accurate assessment of the contribution of the steel core configuration to the overall seismic performance of the bridge piers.

Figure 5 presents the axial–flexural interaction diagram for the three studied sections in the longitudinal direction of the bridge. The CES 1 section demonstrates greater moment resistance in the longitudinal direction compared to the other sections, primarily due to the configuration of the wide-flange steel core, which is aligned along its strong axis. This configuration enhances the overall resistance of the CES 1 section. In addition, it is shown that the three studied columns have a resistance 20% lower than the seismic elastic demand as stated previously.

Figure 6 presents the axial–flexural interaction diagram for the three studied sections in the transverse direction of the bridge. In this direction, the CES 3 section exhibits higher resistance compared to the other sections, as the steel core is oriented in the transversal direction. In addition, it can be seen that the seismic elastic demand is considerably lower than the resistance of the three studied sections. However, the maximum seismic demand in typical bridges is in the longitudinal direction.

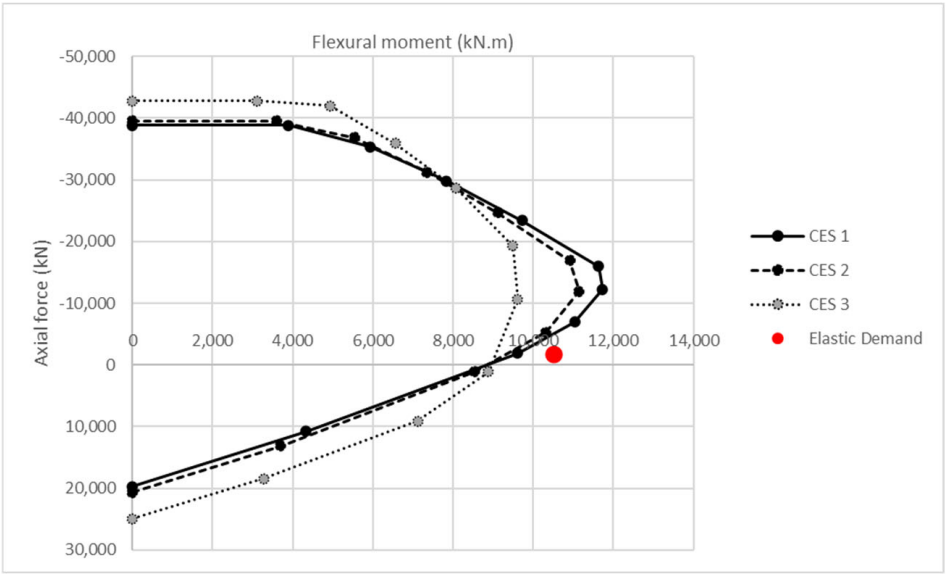

Figure 5. Axial–flexural interaction diagram for the studied section in the longitudinal direction.

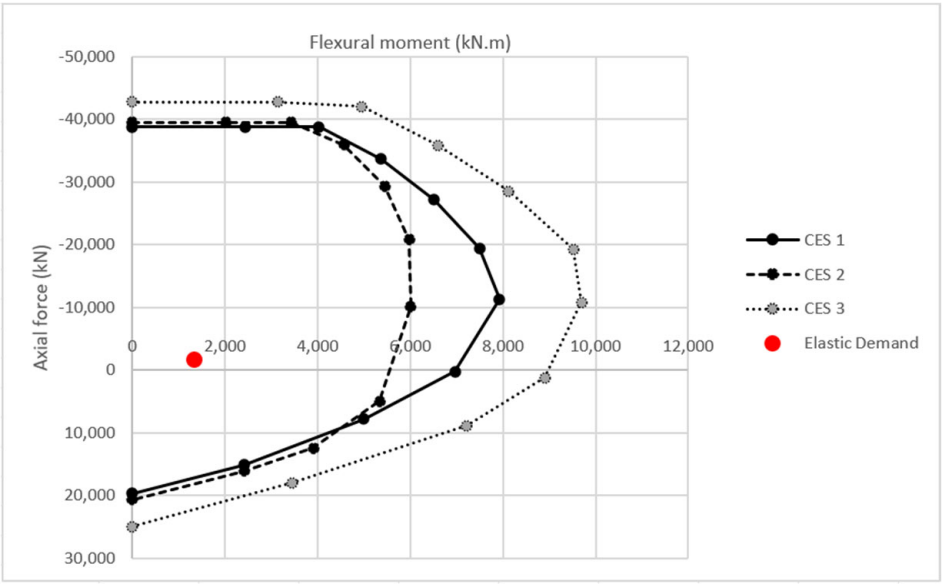

Figure 6. Axial–flexural interaction diagram for the studied section in the transversal direction.

2.1. Numerical Analysis

To better understand the nonlinear behavior of the CES bridge pier section, a fiber-based model was developed using the finite element software CSI Bridge V26 [19], and the seismic performance of the three CES sections was studied.

In the first step, an existing experimental analysis was used for validation to confirm the accuracy of the developed numerical model. The numerical model of the test sample was compared with the experimental results of a rectangular CES column tested by Hsu et al. [22] under cyclic loading conditions. As presented in Figure 7, the experimental results were plotted alongside the force–displacement response derived from the numerical simulation in CSI Bridge software. The comparison shows a strong agreement between the two diagrams, demonstrating the model's accuracy in representing structural behavior. In addition to the visual comparison shown in Figure 7, the numerical model predicted the peak lateral displacement and initial stiffness with deviations lower than 10%, relative to the experimental results, confirming the reliability of the adopted modeling strategy for

nonlinear seismic analysis of CES columns. This validation step reinforces the suggested method's accuracy and suitability for CES columns. However, it should be noted that experimental data for CES bridge columns subjected to cyclic loading remain limited in the literature. Therefore, validation was conducted using the most representative available experimental dataset. Although the obtained agreement confirms the adequacy of the modeling approach, additional experimental validation would further strengthen the general applicability of the model for future research.

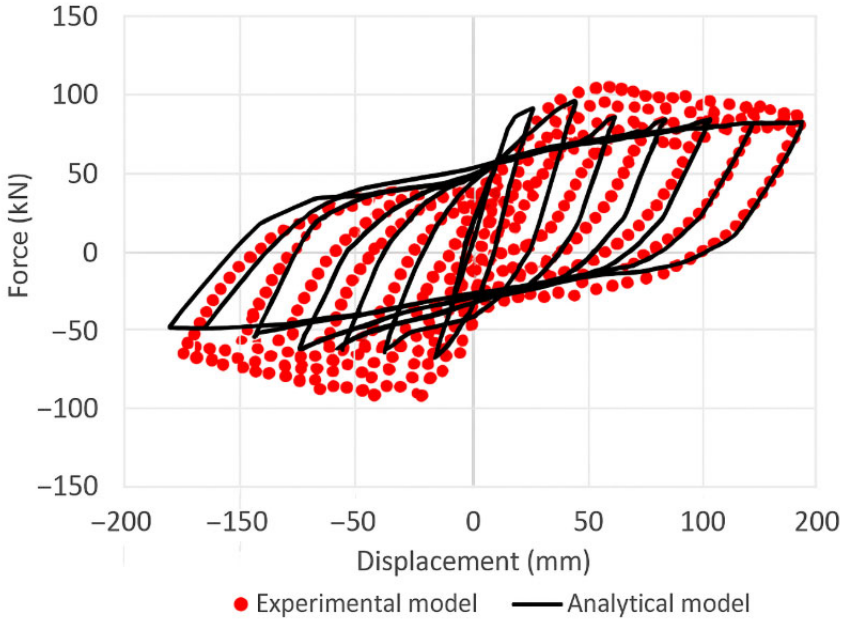

Figure 7. Force–displacement diagram for analytical model from CSI software vs. experimental model (reprinted from [22] with permission from Elsevier).

The CES sections were analyzed using the fiber section model, where the section is divided into "n" fibers of varying sizes. Each CES cross-section was divided into concrete, reinforcement, and structural steel fibers using a sufficiently fine discretization to accurately capture the stress distribution across the section. A sensitivity check was performed by increasing the number of fibers and comparing the results to confirm the adequacy of the adopted fiber discretization. The stresses within these fibers were integrated across the cross-sectional area to determine the corresponding strain actions, such as moment or force. Each steel reinforcing bar, structural steel section, or concrete fiber was assigned specific material properties. Fiber stresses were calculated using the "plane sections remain plane" theory in combination with appropriate constitutive models. Several formulas were used to calculate the strain in the fibers as the loads increase. The section's axial strain and curvature relative to a fixed reference system were described by Spacone et al. [23], and the evolution of the neutral axis (NA) position was not explicitly tracked.

Due to the bending stiffness of the steel flanges, the steel core of the CES section can contribute to the lateral confining pressure of the expanded concrete. The Mander model, initially introduced for reinforced concrete [24], can be applied to highly confined concrete (HCC) in CES columns, provided that the effective lateral confining pressure from the steel core is recognized. As a result, by carefully considering the lateral interaction between the concrete and steel core, a unified stress–strain relationship was established for HCC. The stress–strain relationship of the CES section was described using Chen et al. model [10] as presented in Figure 8.

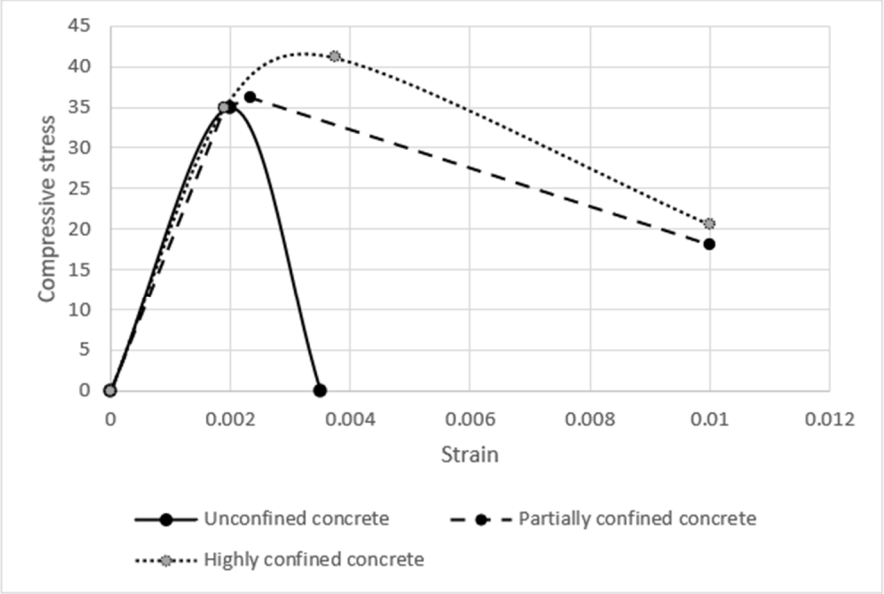

Figure 8. Concrete nonlinear behavior model for the CES section.

2.2. Material Properties

In order to better understand the nonlinear behavior of the CES bridge pier section, a fiber-based model was developed using the finite element software CSI Bridge [19] and the seismic performances of the three CES sections were studied and compared.

The CES sections were analyzed using the fiber section model. The sections were divided up into "n" fibers, which are not necessarily all of the identical size. Stresses were integrated into the cross-section area in order to determine the straining actions, such as moment or force. Each steel reinforcing bar, structural steel section, or concrete fiber has a specific set of material qualities. Fiber stresses were calculated from them using the "plane sections remain plane" theory along with relevant constitutive models. There are several formulas for calculating the strain on the fiber as the loads increase. The section axial strain and curvatures with respect to a fixed reference system were described by [23], and they did not have to monitor the evolution of the neutral axis (NA) position. As presented previously in Figure 9, the concrete section in the CES column's cross-section is divided into three zones, unconfined concrete (UC), partially confined concrete (PCC), and highly confined concrete (HCC).

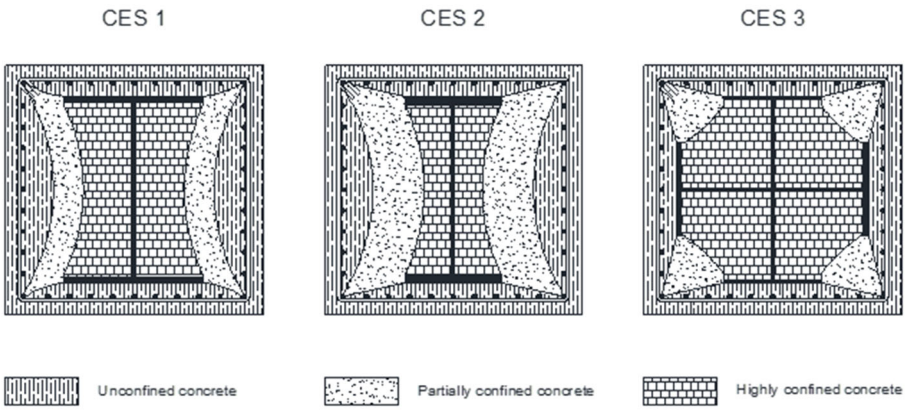

Figure 9. Definition of the confinement zones in CES sections.

Due to the steel flanges' bending stiffness, the steel core of the CES section could contribute to the expanded concrete's lateral confining pressure. The Mander model, first

introduced for reinforced concrete [24], can be applied to HCC in CES columns as long as it is established that the steel core's effective lateral confining pressure exists. Consequently, by closely examining the lateral interaction between the concrete and steel core, a unified stress–strain relation can be provided for HCC.

The stress–strain relationship of the CES section was described using Chen and Wu model [25] as presented in Figure 8.

$$f'_{cc\ p} = K_p.f'_{co} = f'_{co}\left(-1.254 + 2.254\sqrt{1 + \frac{7.94f'_{le,p}}{f'_{co}}} - 2\frac{f'_{le,p}}{f'_{co}}\right) \quad (2)$$

$$f'_{cc\ h} = K_h.f'_{co} = f'_{co}\left(-1.254 + 2.254\sqrt{1 + \frac{7.94f'_{le,h}}{f'_{co}}} - 2\frac{f'_{le,h}}{f'_{co}}\right) \quad (3)$$

As presented in Equations (2) and (3), the confinement factors (K_p and K_h) are the confinement impact for highly and partially confined concrete. Furthermore, $f'_{le,p}$ is the effective confining pressure from stirrups and $f'_{le,h}$ is the effective lateral confining pressure for highly confined concrete.

For rebars and the steel section, the minimum elongation is defined based on [26,27] as presented in Figure 10.

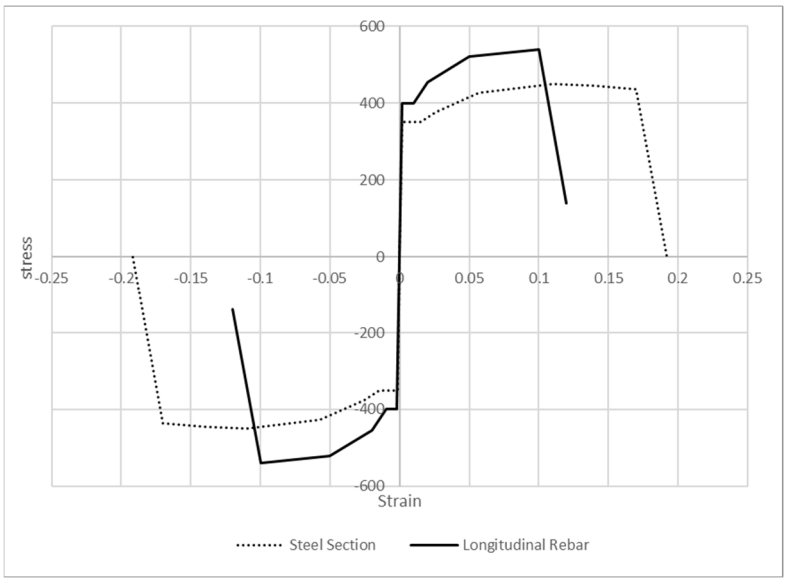

Figure 10. Nonlinear behavior model for the steel section and the longitudinal rebar.

2.3. Pushover Analysis

A pushover analysis was conducted on all the bridge models to determine the displacement capacity and the individual fiber performance of the studied sections. Figure 11 presents a comparative diagram of the longitudinal shear base for the analyzed columns. A comparison of the nonlinear pushover analysis results for the three studied sections reveals that all sections exhibit similar behavior in terms of ductility and shear capacity. However, the CES 1 model demonstrates a more rigid section in the longitudinal direction because of the shape of the wide-flange steel profile section. It should be noted that the yield displacement was determined from the pushover capacity curve, where the yield point corresponds to the intersection between the initial elastic stiffness line and the horizontal line representing the effective yield strength. Based on this procedure, the yield displacements were approximately 54 mm, 50 mm, and 45 mm for the CES 1, CES 2, and CES 3 sections, while the displacement demand, based on spectral analysis, was 34 mm.

This indicates that the elastic displacement capacity of all studied sections is greater than the design displacement demand, confirming that all sections have an elastic response under the design earthquake for the studied zone.

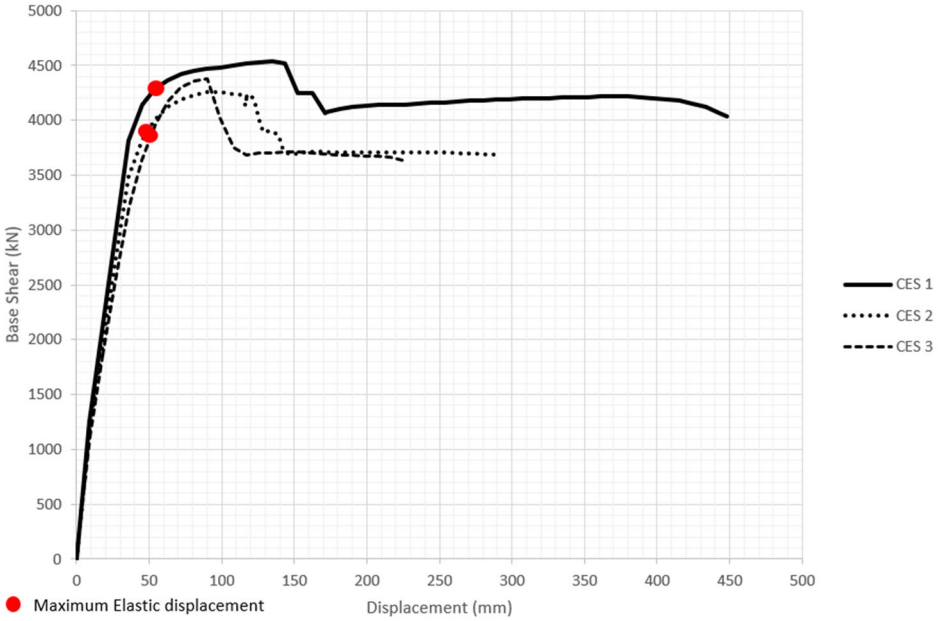

Figure 11. Longitudinal base shear vs. displacement diagram for studied CES sections.

In addition, the analysis shows that the section CES 1 has a better ductile behavior than the other studied sections. The ductility in CES 1 section is approximately 9.0, while the ductility in section CES 2 and section CES 3 are 6.0 and 4.0 respectively. Moreover, section CES 1 seems to have a better rigidity compared to the other studied sections. A fiber model was developed to capture the behavior of unconfined concrete, partially confined concrete, highly confined concrete, and reinforcement steel in the studied sections. The concrete cover was modeled as unconfined concrete. The analysis indicates that the concrete cover experiences cracking under tensile behavior for a displacement corresponding to the design displacement. However, it does not spall under compression in any of the studied columns. Additionally, no plastic behavior was observed in the steel reinforcement under the design displacement in any of the sections. It is important to note that the failure of the partially confined concrete is considered as the ultimate state representing the failure of the three studied sections. When the partially confined concrete fails, the confinement around the rebar loses effect and fails to carry load in the CES section.

Figures 12 and 13 show the stress displacement behavior of the partially confined concrete and highly confined concrete, respectively, for the CES 1 section. It can be observed that at the design displacement of the bridge, both partially and highly confined concrete have a linear behavior. A similar behavior was observed for the CES 2 and CES 3 sections. In addition, the failure of the partially and highly confined concrete reaches a bridge displacement of approximately 440 mm, which shows a ductility ratio of approximately 9. Figure 14 shows the stress displacement behavior in compression of the unconfined concrete for the CES 1 section. It can be concluded that at the design displacement of the bridge, the unconfined concrete has not reached failure yet, which is the same behavior as the CES 2 and CES 3 sections. Moreover, Figure 14 shows the stress displacement behavior in compression of the unconfined concrete next to the steel flange. It can be concluded that the unconfined concrete next to the steel flange reaches failure at 170 mm displacement of the deck, which is greater than the design displacement of the bridge.

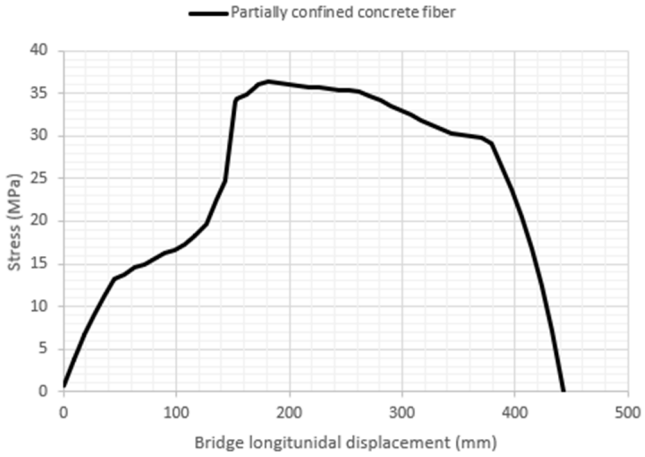

Figure 12. Partially confined concrete compression stress–strain diagram for the CES 1 section.

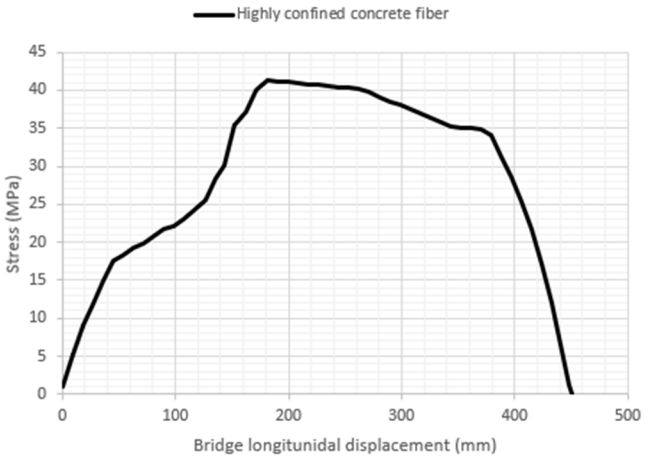

Figure 13. Highly confined concrete compression stress–strain diagram for the CES 1 section.

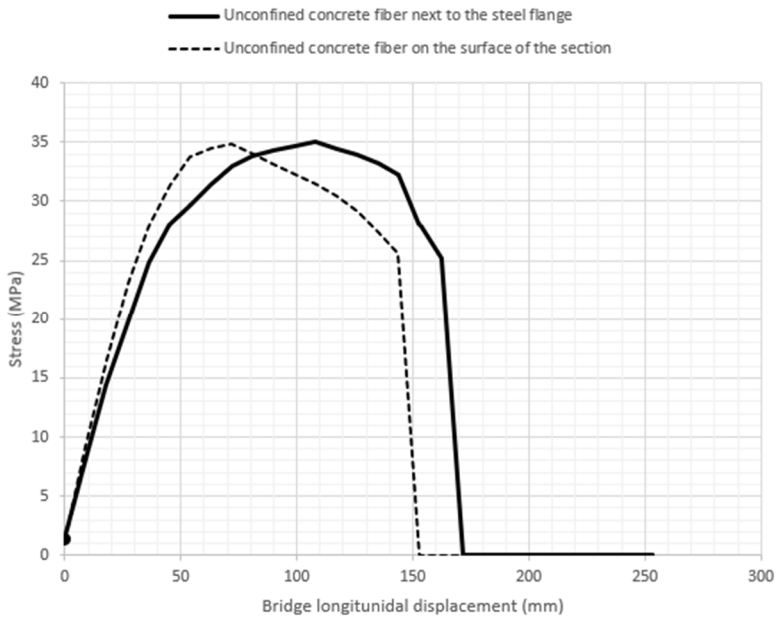

Figure 14. Unconfined concrete compression stress–strain diagram for the CES 1 section.

Figure 15 shows the stress displacement behavior for the steel flange in tension and compression for the CES 1 section. It is shown that the capacity displacement of the steel

flange in tension and in compression is greater than the design displacement, similarly to the CES 2 and CES 3 sections.

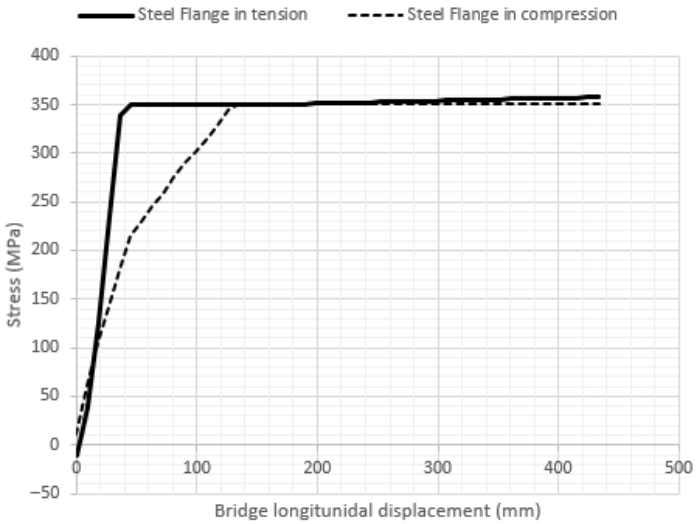

Figure 15. Steel flange tension and compression stress displacement diagram for the CES 1 section.

2.4. Nonlinear Time-History Analysis

Nonlinear time-history analyses were carried out using the two orthogonal principal components of the selected earthquakes as input to simulate the nonlinear seismic response of the models under the scaled earthquakes. Time-history analysis aims to assess the performance and compare the nonlinear behavior of the column under an extreme event representing a seismic event with a 2% in 50 years return period, which represents the uniform hazard spectra for a lifeline bridge design according to the CHBDC [17] requirements.

2.4.1. Selection of the Ground Motion Records

The tectonic regime, magnitudes, and distances that influence the seismic hazard at a particular location should all be taken into account when selecting appropriate ground motions. According to the CHBDC [17], dynamic analysis requires an ensemble with a minimum of eleven ground motion time records. Ground motions should consist of pairs of appropriate horizontal ground motion components when the analysis is carried out with orthogonal horizontal ground motion time histories applied simultaneously. If possible, pairs of horizontal ground motion components captured at the same location during the same event are usually employed for this. For some applications, this can also be done with a set of two statistically independent simulated ground motions created for the identical M-R and fault conditions [28].

The seismic activity in Eastern Canada is moderate, and there are not many ground motion records from earthquakes that are consistent with the danger level that the CHBDC [17] has chosen. In the present study, fifteen pairs of ground motion records were used, containing five historical ground motion records in Eastern Canada and ten pairs of simulated ground motions created by Atkinson [28]. The selection and number of ground motion records were determined in accordance with the seismic analysis recommendations of the Canadian Highway Bridge Design Code issued by the CSA Group. The CHBDC [17] recommends the use of a minimum of 11 ground motion records for nonlinear time-history analysis to ensure statistically reliable response estimates. In the present study, a total of 15 ground motion records were adopted, exceeding the minimum code requirement and improving the statistical robustness of the analysis. The record selection and scaling procedures were carried out following the methodology described in ref. [26], which are widely used in engineering practice and research for representing seismic hazard con-

ditions in Eastern Canada. This approach ensures that the adopted dataset provides an appropriate representation of regional seismic characteristics while satisfying accepted Canadian seismic analysis practices. As suggested by Tremblay et al. [29], the mean value of the largest five response values of an ensemble of 15 records composed of three suites of five records represents a maximum value of the performance evaluation. Therefore, five ensembles of historical ground motions recorded in Eastern Canada were selected based on the seismic hazard at Montreal. Each earthquake record includes two orthogonal horizontal components. The properties of the selected ground motion earthquakes used in this study are presented in Table 2, along with the orientation of the recorded historical and simulated ground motion horizontal components.

Table 2. Properties of the non-scaled selected ground motion records.

Record No.	Date, Event	Mw	R (km)	Component, Orientation	PGA (g)
NHN_BC1	23 December 1985, Nahanni	6.5	24	Bettlement Creek-S3, N 270	0.186
NHN_BC2				Bettlement Creek-S3, N 360	0.194
OTT_R1	23 June 2010, Ottawa	5.0	58.7	Val-des-Bois-NS	0.034
OTT_R2				Val-des-Bois-EW	0.033
SAG_CN1	25 November 1988, Saguenay	5.7	43	Chicoutimi Nord, N 124	0.131
SAG_CN2				Chicoutimi Nord, N 214	0.106
SAG_EB1	25 November 1988, Saguenay	5.7	90	Les Eboulements, NS 0	0.125
SAG_EB2				Les Eboulements, EW 270	0.102
SAG_SA1	25 November 1988, Saguenay	5.7	64	Saint-Andre, NS 0	0.156
SAG_SA2				Saint-Andre, EW 270	0.091
6c-1-x	Simulated	6.0	12.8	x	0.352
6c-1-x				y	0.405
6c-2-x	Simulated	6.0	17.0	x	0.397
6c-2-x				y	0.392
6c-3-x	Simulated	6.0	17.0	x	0.271
6c-3-x				y	0.300
6c-4-x	Simulated	6.0	30.7	x	0.198
6c-4-x				y	0.138
6c-5-x	Simulated	6.0	24.8	x	0.183
6c-5-x				y	0.141
7c-1-x	Simulated	7.0	25.2	x	0.386
7c-1-x				y	0.314
7c-2-x	Simulated	7.0	25.7	x	0.327
7c-2-x				y	0.289
7c-3-x	Simulated	7.0	25.6	x	0.329
7c-3-x				y	0.311
7c-4-x	Simulated	7.0	100.2	x	0.085
7c-4-x				y	0.088
7c-5-x	Simulated	7.0	98.6	x	0.078
7c-5-x				y	0.142

2.4.2. Transformation and Scaling of Ground Motions

In order to preserve the original signature and energy distribution of the ground motions, the NBCC Guidelines recommend using simple linear scaling. It is not advised to use frequency-domain and time-domain spectral matching methods for nonlinear structural analysis unless they are designed to closely match the target spectrum. Therefore, the two horizontal orthogonal components of the selected historical earthquakes were scaled to a 2%/50 years return period of the uniform hazard spectra (UHS), for a site condition representative of site class C, using a spectral matching technique in the time domain [30]. The two resultant spectra were then separated by scaling the response spectra up and down by the factors of 1.125 and 0.844 to achieve a spectral ratio of the minor to the major component

of 0.75 [31,32]. The 5% damped absolute acceleration response spectra of the major and minor ground motion components are presented in Figures 16 and 17 respectively.

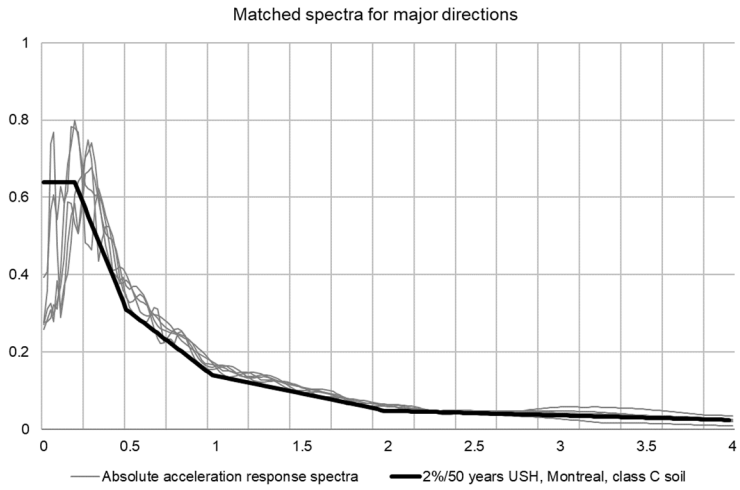

Figure 16. Matched response spectra of the selected earthquake records in major directions.

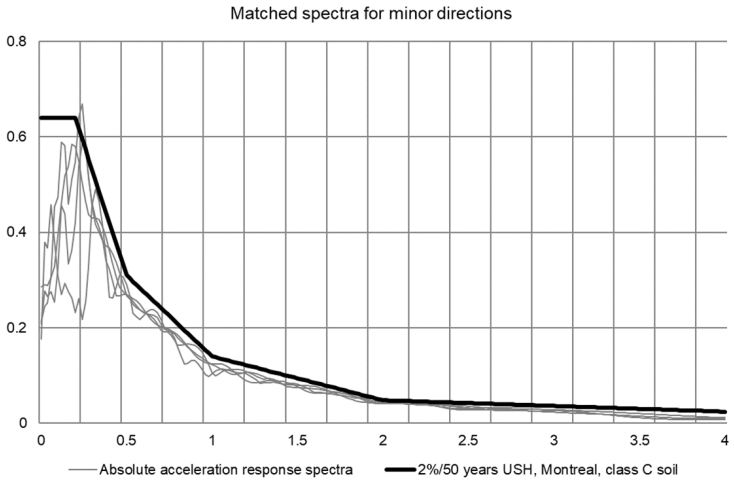

Figure 17. Matched response spectra of the selected earthquake records in minor directions.

The period range for matching the acceleration with the uniform hazard spectra was calculated as suggested by [29]. The lower limit of the period range, T_{min}, is considered the minimum value of the period of the highest vibration mode required to cumulate a minimum participating mass of 90% of the structure mass and 0.2 times the fundamental period of the structure. In addition, the upper limit of the period range, T_{max}, is considered equal to maximum value between two times the fundamental period of the structure and 1.5 s. Therefore, the period range for ground motion selection and scaling purposes is defined as presented in Equations (4) and (5) and considered equal to 0.15 s for T_{min} and 1.8 s for T_{max}.

$$T_{min} = min(0.2T_1;\ T_{90\%}) \quad (4)$$

$$T_{max} = max(2.0T_1; 1.5\ \text{s}) \quad (5)$$

2.4.3. Time-History Analysis

Maximum fiber strains represent an excellent indicator and comparison parameter of the damage level associated with each case. For example, they are directly compared with the performance criteria presented in the Canadian Highway Bridge Design Code (CHBDC) [17], allowing to classify the damage severity level for each studied bridge

column section and to assess thereby the effect of the steel reinforcement configuration. Table 3 presents the maximum strains obtained for the unconfined concrete cover, partially confined concrete, highly confined concrete, corner longitudinal rebar and the steel core section, within the column's plastic hinge regions of the CES 1 section under the selected ground motions scaled to the uniform hazard spectra of 2% probability of occurrence over 50 years.

Table 3. Maximum strains in CES 1 columns under the design ground motions.

Seismic Records	Rebar Reinforcement $\times 10^{-3}$ (Tension)	Steel Core $\times 10^{-3}$ (Tension)	Concrete Cover $\times 10^{-3}$ (Compressive)	Partially Confined Concrete $\times 10^{-3}$ (Compressive)	Highly Confined Concrete $\times 10^{-3}$ (Compressive)
Historical records	1.91	1.55	1.21	0.88	0.70
Artificial records 6c	5.34	4.66	2.62	1.76	1.36
Artificial records 7c	5.74	4.99	2.75	1.77	1.36
Maximum	5.74	4.99	2.75	1.77	1.36

Furthermore, the maximum strains obtained for the unconfined concrete cover, partially confined concrete, highly confined concrete, corner longitudinal rebar and the steel core section, within the column's plastic hinge regions of the CES 2 and the CES 3 section for the 2% in 50 years uniform hazard spectra, are shown in Tables 4 and 5.

Table 4. Maximum strains in CES 2 columns under the design ground motions.

Seismic Records	Rebar Reinforcement $\times 10^{-3}$ (Tension)	Steel Core $\times 10^{-3}$ (Tension)	Concrete Cover $\times 10^{-3}$ (Compressive)	Partially Confined Concrete $\times 10^{-3}$ (Compressive)	Highly Confined Concrete $\times 10^{-3}$ (Compressive)
Historical records	2.12	1.67	1.41	1.00	0.70
Artificial records 6c	5.29	4.35	2.41	1.56	1.12
Artificial records 7c	5.07	4.35	2.44	1.60	1.21
Maximum	5.29	4.35	2.44	1.60	1.21

Table 5. Maximum strains in CES 3 columns under the design ground motions.

Seismic Records	Rebar Reinforcement $\times 10^{-3}$ (Tension)	Steel Core $\times 10^{-3}$ (Tension)	Concrete Cover $\times 10^{-3}$ (Compressive)	Partially Confined Concrete $\times 10^{-3}$ (Compressive)	Highly Confined Concrete $\times 10^{-3}$ (Compressive)
Historical records	1.94	1.64	1.32	0.93	0.73
Artificial records 6c	4.28	3.39	2.58	1.82	1.42
Artificial records 7c	4.03	3.36	2.33	1.53	1.33
Maximum	4.28	3.39	2.58	1.82	1.42

According to the obtained results presented in Tables 3–5, concrete compressive strains in all studied sections are lower than 0.0035, which is lower than the limit for spalling. However, reinforcing steel strain is greater than the yield limit, which is equal to 0.002 with more potential damage to the steel rebars in CES 1 sections than that in CES 2 and CES 3 sections, which can be explained by the steel ratio in the studied sections. Furthermore, based on the tensile strain in the steel, the tensile strain in all studied sections shows that the concrete is cracked in tensile areas. It can be seen that all studied sections have a similar seismic performance, which meets the seismic performance requirements of a lifeline bridge according to the CHBDC [17].

Figure 18 shows the stress–strain diagrams of the three studied sections for the unconfined concrete fiber under 6C-4 seismic records. It can be concluded that the unconfined concrete behaves slightly differently when the steel configuration inside the concrete-encased steel sections changes. CES 1 has a more stable curve with medium stiffness and strength. CES 2 shows more variation and instability, which means it is less ductile when strain increases. Even if the behaviors are slightly different, all three sections reach the same level of damage according to the CHBDC [17]. This means that the final damage condition is not strongly affected by the steel configuration, even if the stiffness and ductility are slightly different.

Figure 19 presents the stress–strain diagrams of the three studied sections for partially confined concrete fiber under 6C-4 seismic records. Some differences in behavior depending on the steel configuration in the studied sections can be observed. It is shown that CES 1 presents higher stiffness and reaches the peak strength more quickly. Even if the curves are slightly different, all three sections reach the same level of damage according to the CHBDC [17]. This means that the final damage limit is similar for all configurations, even if their stiffness and ductility are not exactly the same.

Figure 20 presents the stress–strain diagrams of the three studied sections for highly confined concrete fiber under 6C-4 seismic records. It shows the confinement effect due to the steel configuration inside the CES sections. As it was observed for the partially confined concrete, CES 1 develops high stiffness and reaches the maximum strength at low strain while CES 2 and CES 3 show a more gradual response, with less stiffness. Even if the curves are slightly different, all three sections reach the same damage level according to the CHBDC [17]. This shows that the confinement increases stiffness and ductility, but the final damage limit is the same for all configurations.

The comparison of the stress–strain diagrams for unconfined, partially confined, and highly confined concrete in the three sections shows how the level of confinement changes the behavior of the section. The unconfined concrete presents lower stiffness, larger variation, and faster strength loss after the peak. The partially confined concrete shows better stability and higher strain capacity, with slower degradation compared to the unconfined case. The highly confined concrete has the best performance, with greater stiffness, higher ductility, and longer energy absorption before failure. Even if the shapes of the curves are different in each of the studied sections, all three sections reach the same final damage condition according to the CHBDC [17]. This means that confinement improves stiffness and ductility, but the code damage limit remains the same for all studied configurations.

Figure 21 presents the stress–strain diagram for the longitudinal rebar for all studied sections under 6C-4 seismic records. Figure 21 show similar overall behavior with some small differences depending on the steel configuration. In general, all three sections reach high stress values to the yield strength of the reinforcement and maintain this level over a wide strain range. It can be concluded that CES 1 shows a more regular curve with good stiffness. Even if the details of the curves are different, the global behavior of the

longitudinal rebars is consistent, showing that the steel reinforcement provides stable strength and ductility across all CES configurations. It is shown that while the steel profile fiber reaches the yield point, the strain level stays below the repairable damage according the performance criteria levels described in the CHBDC [17]. The maximum strain is 0.005738 versus the CHBDC [17] performance criteria limit 0.01.

Figure 22 presents the stress–strain diagram for the steel profile section for the CES section under 6C-4 seismic records. The stress–strain diagrams of the steel profiles in the three CES sections show a very consistent behavior across the different configurations. All profiles reach high stress values to the yield strength and keep this level over a wide strain range, which demonstrates good ductility. CES 1 shows a slightly steeper slope at the beginning, indicating higher initial stiffness. Even with these small differences, the global response of the steel profiles remains very similar, confirming that the steel section provides reliable strength and ductility regardless of the specific CES configuration. It is also shown that while the steel profile fiber reaches the yield point, the strain level stays below the repairable damage according the performance criteria levels described in the CHBDC [17]. The maximum strain is 0.002975 versus the CHBDC [17] performance criteria limit of 0.01. The comparison of the stress–strain responses indicates that CES 1 exhibits slightly higher initial stiffness and improved confinement effectiveness due to the orientation of the wide-flange section along the primary bending direction. CES 2 and CES 3 present more gradual stiffness degradation, reflecting differences in confinement distribution and steel–concrete interaction. Despite these variations, all configurations maintain stable post-yield behavior and reach comparable ultimate performance levels according to CHBDC [17] performance criteria.

Figures 23 and 24 present the base shear versus drift ratio diagrams for all three CES sections under 6C-4 and 7C-2 seismic records. Each selected records represents the most critical performance of the selected group of five records presented beforehand. The base shear–drift ratio diagrams of the three CES sections under synthetic seismic records show very similar overall shapes, with only small variations related to the steel configuration. All three sections present high lateral resistance and maintain stable hysteresis loops throughout seismic loading. The comparison between three studied section shows that CES 1 exhibits slightly higher initial stiffness at small drift ratios. Despite these differences, the three CES systems achieve a comparable global performance level under seismic loading, which confirms that alternative steel configuration in the composite section led to similar structural resistance when subjected to seismic events.

In general, based on the results of the nonlinear time-history analysis of the CES sections, the stress displacement analysis of the bridge shows that fiber responses in both partially and highly confined concrete stay below the seismic demand levels. Fibers in highly confined concrete experience less strains and show a better performance. However, those in partially confined areas still behave acceptably with slightly more deformation. When compared to the ultimate deformation capacity from the pushover analysis, the bridge stays within its seismic demand. For site class C, where ground motions are less intense, the absence of damage suggests the section might be overdesigned, offering a generous safety margin. In contrast, for site class D with softer soils, the demands get closer to the section's capacity, which might justify a closer look at the design. In general, deformation capacity plays a major role in whether a section ends up being overdesigned, especially when ductility goals are set higher than what the seismic demand actually requires.

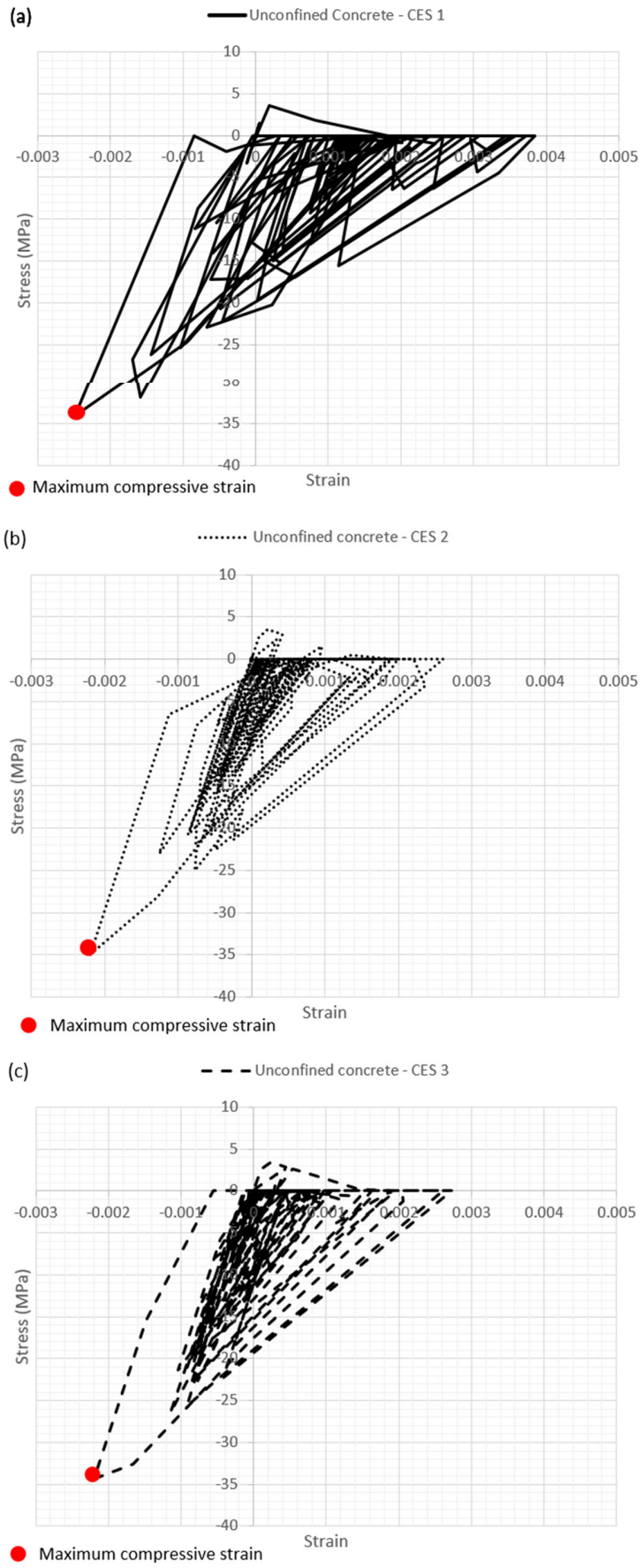

Figure 18. Stress–strain diagrams for the unconfined concrete under 6C-4 seismic records for studied sections: (**a**) CES 1, (**b**) CES 2 and (**c**) CES 3.

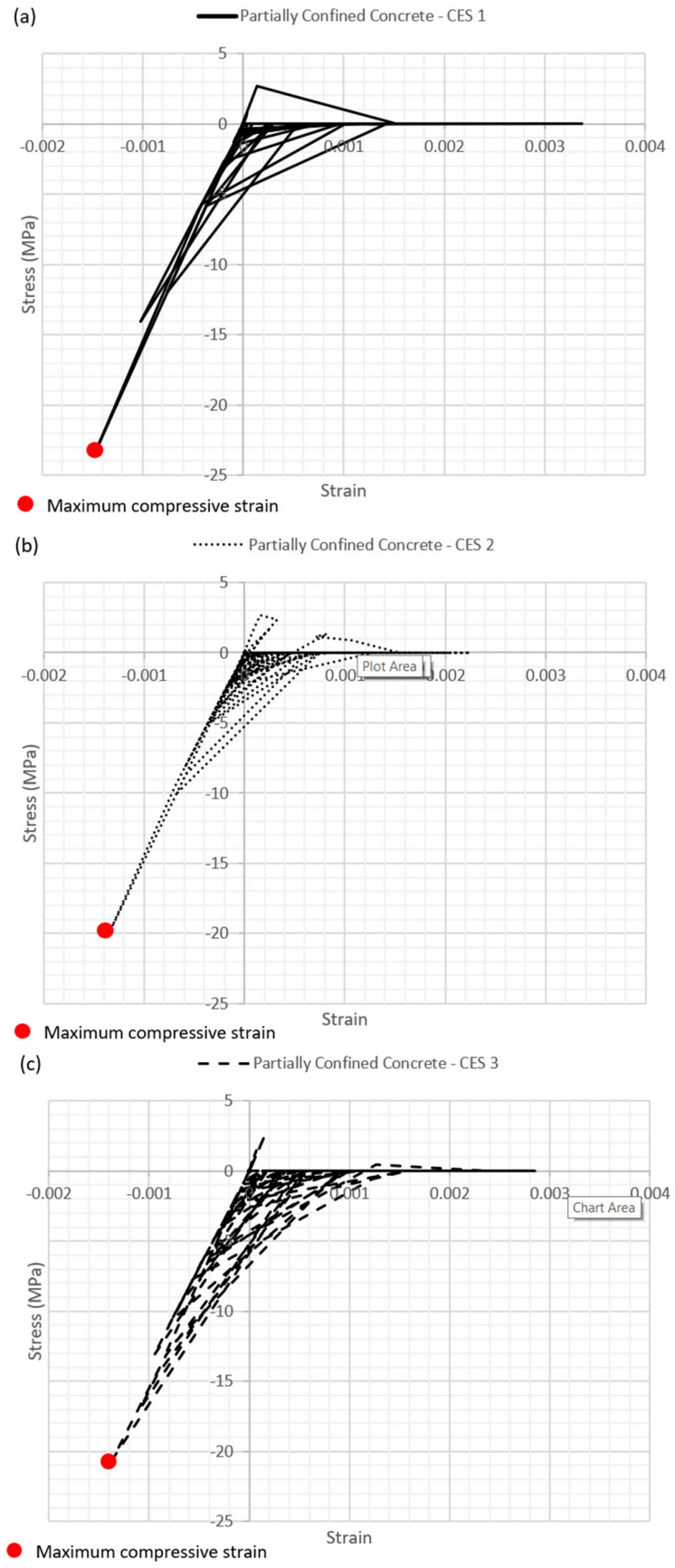

Figure 19. Stress–strain diagrams for the partially confined concrete under 6C-4 seismic records for studied sections: (**a**) CES 1, (**b**) CES 2 and (**c**) CES 3.

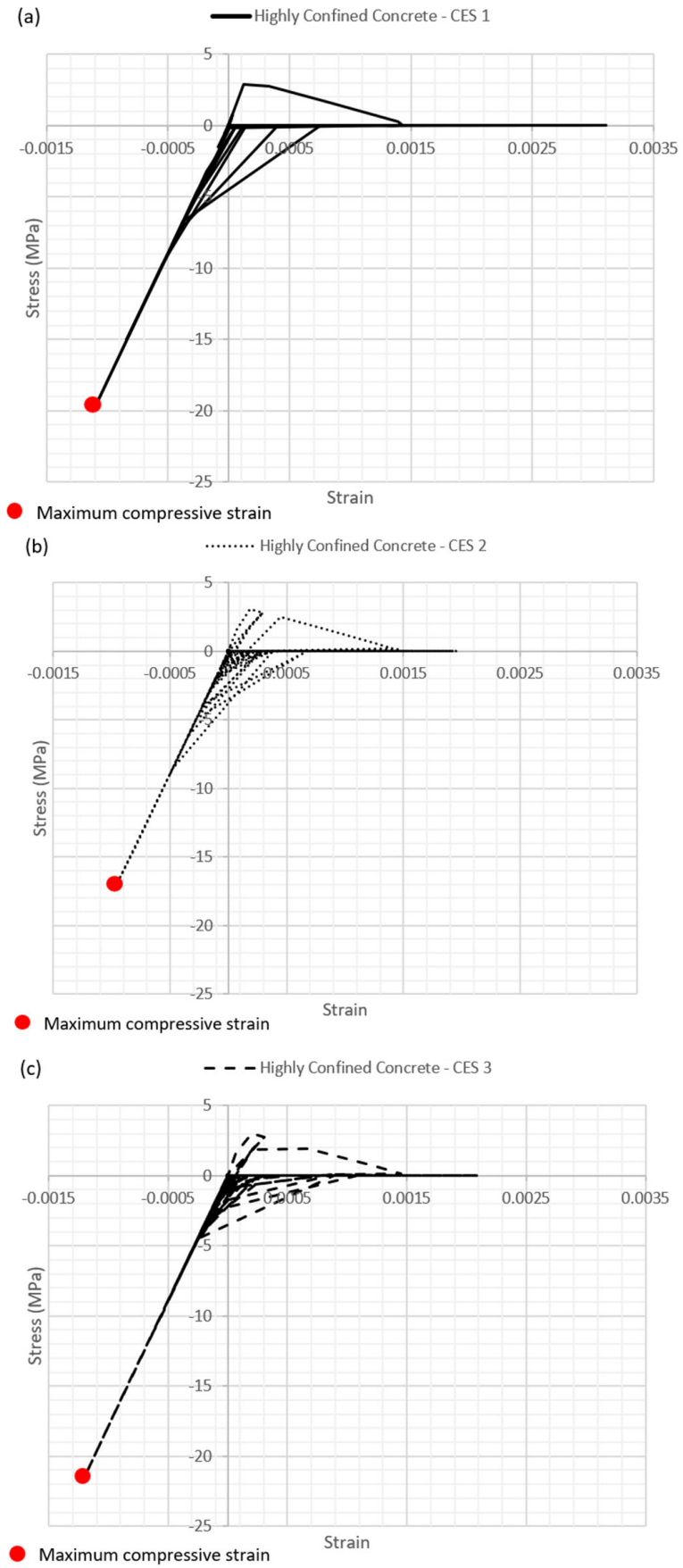

Figure 20. Stress–strain diagrams for the highly confined concrete under 6C-4 seismic records for studied sections: (**a**) CES 1, (**b**) CES 2 and (**c**) CES 3.

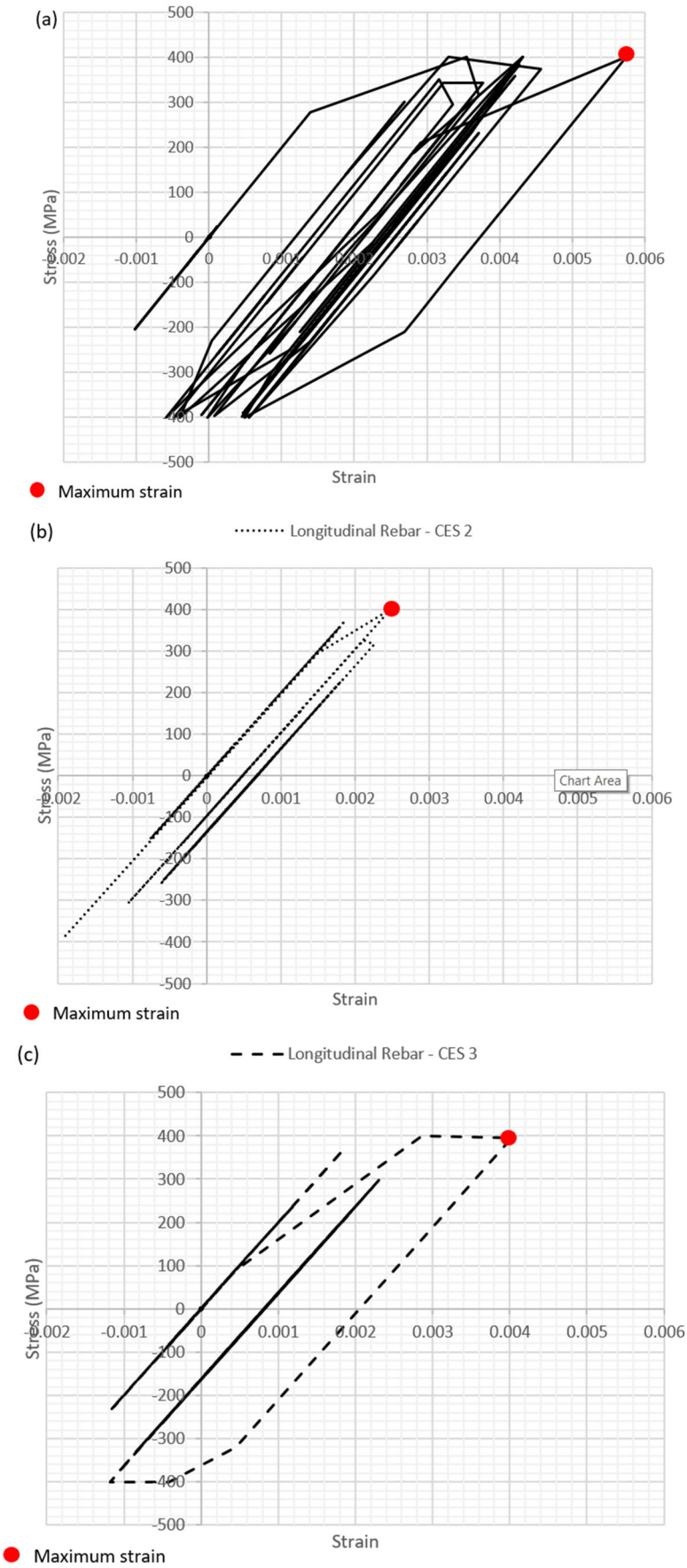

Figure 21. Stress–strain diagram for the longitudinal rebar under 6C-4 seismic records for studied sections: (**a**) CES 1, (**b**) CES 2 and (**c**) CES 3.

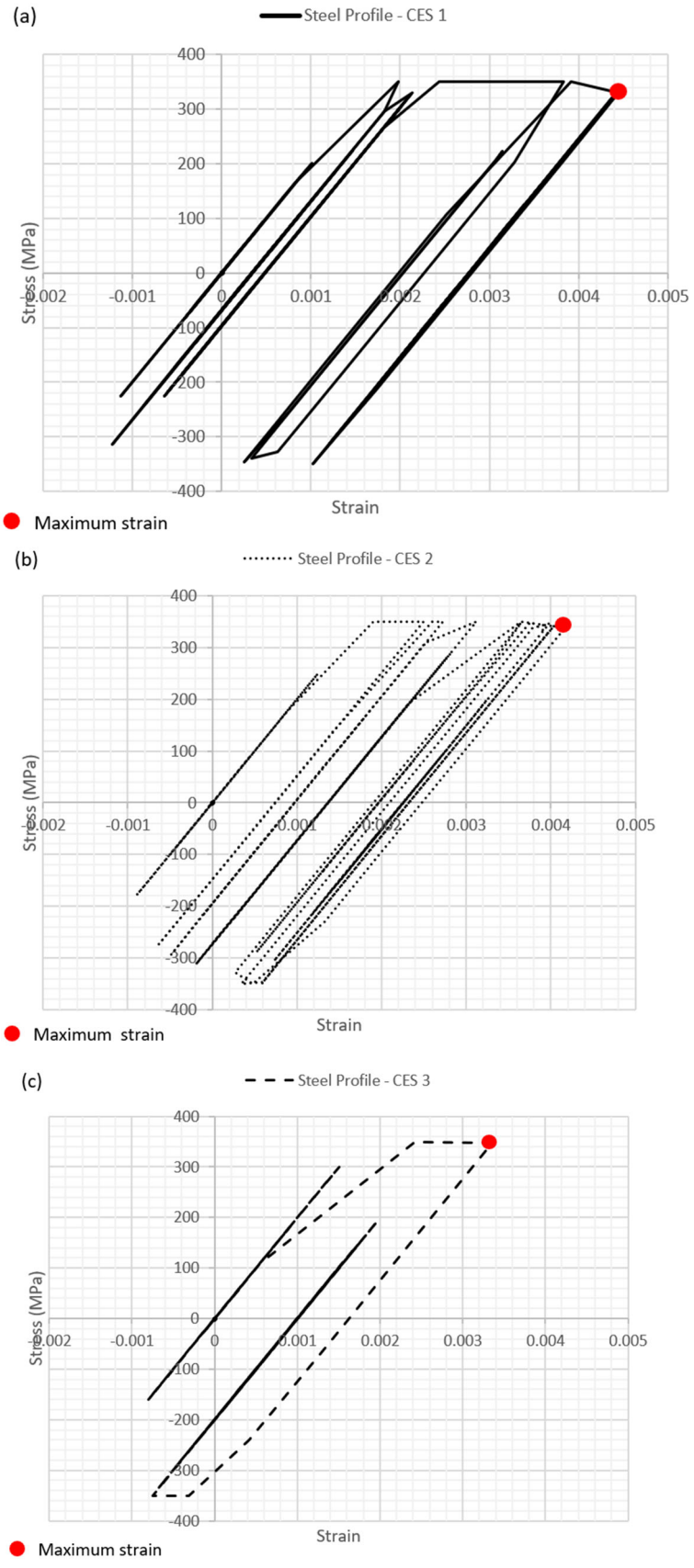

Figure 22. Stress–strain diagram for the steel core section under 6C-4 seismic records for studied sections: (**a**) CES 1, (**b**) CES 2 and (**c**) CES 3.

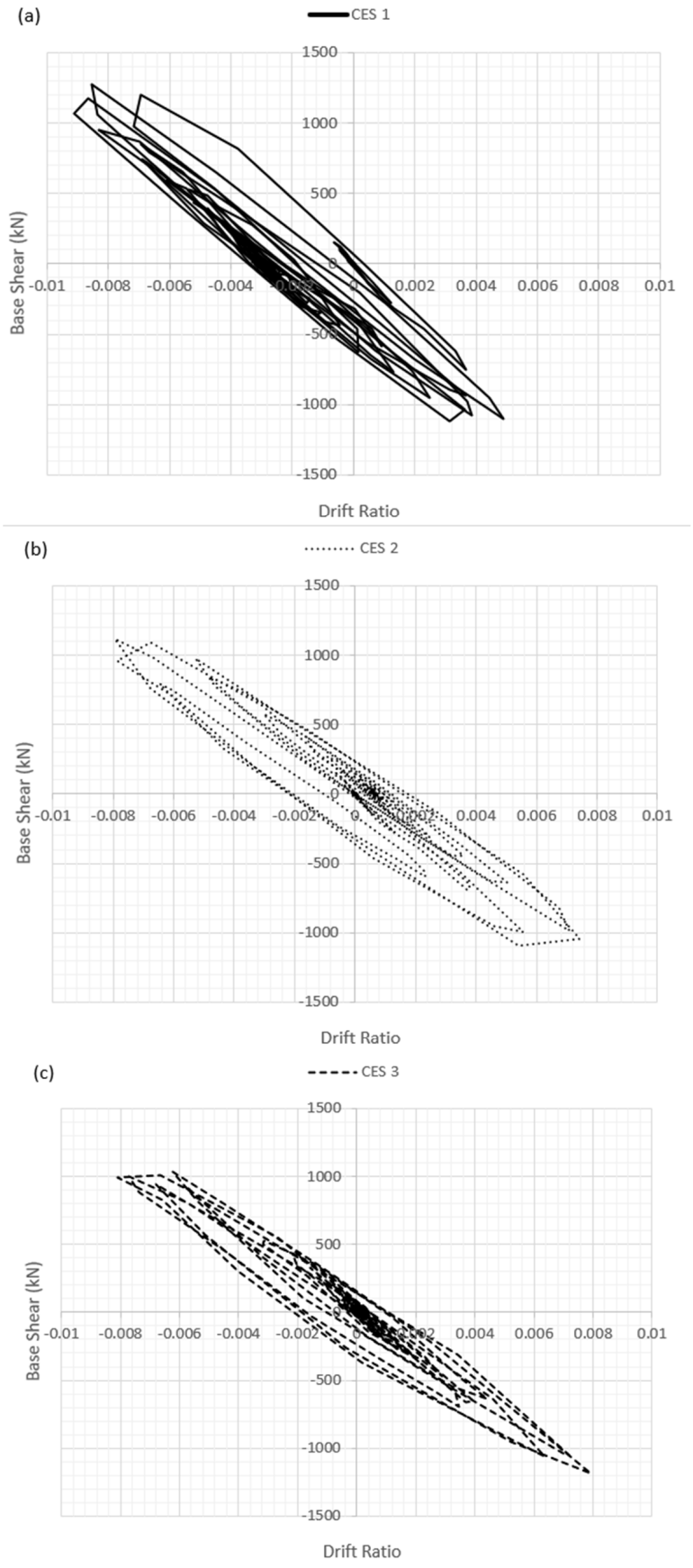

Figure 23. Base shear versus drift ratio diagram for studied sections under 6C-4 seismic records: (**a**) CES 1, (**b**) CES 2 and (**c**) CES 3.

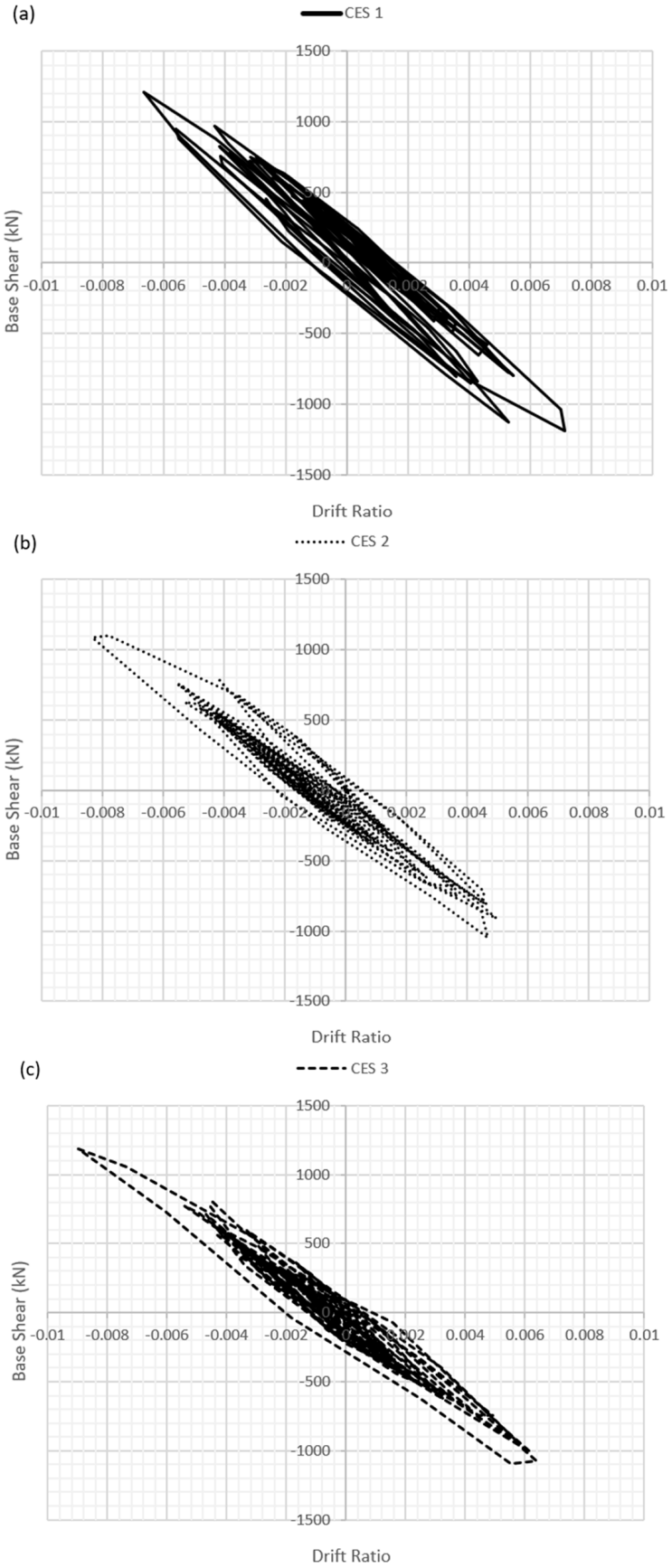

Figure 24. Base shear versus drift ratio diagram for studied sections under 7C-2 seismic records: (**a**) CES 1, (**b**) CES 2 and (**c**) CES 3.

3. Discussion

The comparison of the three CES bridge pier sections shows that all of them behave well under seismic loading and meet the CHBDC [17] requirements. The general failure pattern is similar for all sections, which means the CES piers mainly fail in bending and show stable and ductile behavior during earthquakes. However, the results also show that the steel section configuration has an important effect on the seismic performance. Among the three cases, the CES 1 section performs better overall. The wider-flange steel section provides better confinement to the concrete and higher resistance when the earthquake demand increases. This helps the pier to carry larger forces and deformations before serious damage occurs. The results suggest that a balanced steel design is needed to achieve good seismic performance while keeping durability and practical design considerations.

The obtained results are consistent with previously reported analytical and experimental investigations indicating that the presence and configuration of the structural steel core significantly influence the confinement effectiveness and flexural resistance of CES columns. The improved performance observed for sections incorporating wider flange elements aligns with earlier findings showing that an enhanced steel section increases both stiffness and energy dissipation capacity.

The superior seismic response observed for the CES 1 configuration can be attributed to the alignment of the wide-flange steel section along the primary bending direction, which enhances flexural stiffness, moment capacity, and confinement effectiveness within the plastic hinge region. From a practical perspective, the selection of steel configuration must also consider constructability, fabrication simplicity, and cost efficiency. While larger steel sections may improve seismic resistance, they may also increase fabrication complexity and reduce available concrete cover, which is critical for corrosion protection in regions exposed to severe winter conditions and de-icing salts. Therefore, the final selection of CES configuration should balance seismic performance, durability, and construction practicality.

It should be noted that the conclusions presented in this study are limited to the investigated CES configurations, steel ratios, column geometry, and selected ground motion set. Additional parameters such as axial load ratio, aspect ratio, material strength variations, and higher seismic hazard levels were not included in the present parametric investigation and may influence the relative performance of the studied sections. Therefore, further experimental and analytical studies covering a broader range of design parameters are recommended before establishing generalized design recommendations for CES bridge piers.

4. Conclusions

In this study, a comparative analysis was conducted on three concrete-encased steel (CES) bridge piers, each with a different steel section configuration, to evaluate their relative seismic performance. The three configurations were assessed based on their structural behavior, including seismic response, strength, and overall efficiency in meeting the seismic design requirements of a lifeline bridge according to the CHBDC [17]. The results show that the general performance is stable and the damage level is acceptable for all columns according to the CHBDC [17]. The obtained results are consistent with previously reported analytical and experimental investigations indicating that the presence and configuration of the structural steel core significantly influence the confinement effectiveness and flexural resistance of CES columns. The improved performance observed for sections incorporating wider flange elements aligns with earlier findings showing that an enhanced steel section increases both stiffness and energy dissipation capacity. It should be noted that the conclusions presented herein are based on the investigated parameter range and selected ground motion set, and additional studies considering other parameters such as

axial load ratio, aspect ratio, and material strength variations may further influence the comparative performance.

Furthermore, comprehensive studies including pushover analysis and nonlinear time-history analysis have been performed to assess the seismic behavior of the three CES sections. The findings reported herein support the following conclusions:

- The failure modes of all studied sections are similar. Concrete cracking, longitudinal rebar yielding, unconfined concrete spalling, partially and highly confined failure, longitudinal rebar fracture and steel profile fracture were observed. The observed failure mode represents typical flexural failure in bridge columns.
- The ductility ratios obtained from pushover analysis ranged approximately between 4.0 and 9.0 depending on the steel configuration, which is greater than the minimum ductility ratio specified by the CHBDC [17]. These values demonstrate adequate deformation capacity and confirm that the damage levels remain within acceptable performance limits defined by CHBDC [17].
- The results showed that while all three CES section configurations exhibited a ductile behavior, the best overall seismic performance was for the CES 1 section. The configuration with the wide-flange steel profile optimized for maximum resistance and better confinement demonstrated superior behavior under seismic loading. This configuration resulted in improved structural integrity, higher resistance to bending and shear forces, and better overall performance under extreme seismic events.
- The comparison of the obtained strain demands with CHBDC [17] performance limits confirms that all studied sections satisfy the repairable-damage criteria for lifeline bridges. These limits provide a conservative benchmark for performance-based design, ensuring that bridge columns maintain structural integrity and serviceability following extreme seismic events with a 2% in 50 years return period. The results indicate that CES bridge piers designed using the investigated configurations can meet these code-based performance objectives while providing additional deformation capacity beyond the minimum required limits.
- The comparison of stress–strain diagrams for unconfined, partially confined, and highly confined concrete shows that higher confinement increases stiffness, ductility, and energy absorption, yet all three sections ultimately reach acceptable final damage level according to the CHBDC [17].
- The longitudinal rebars in all CES sections under seismic records reach yield stresses with stable strength and ductility, with minor differences in stiffness, uniformity, and strain capacity, while the maximum strain remains below the CHBDC [17] repairable-damage limit.
- The steel profiles in all CES sections under seismic records reach yield stresses with good ductility and similar overall behavior, with minor differences in initial stiffness and strain capacity, while the maximum strain remains well below the CHBDC [17] repairable-damage limit.
- Based on the comparative analytical study on three CES sections, sections incorporating wide-flange steel cores oriented along the primary bending direction demonstrated better rigidity, moment capacity, and ductility. The results suggest that moderate increases in flange width combined with controlled web thickness provide an effective balance between confinement efficiency, structural capacity, and durability requirements. These findings may serve as preliminary guidance for performance-based design of CES bridge piers until more detailed codified provisions become available.
- Among the investigated configurations and parameter ranges considered in this study, the CES 1 section demonstrated comparatively improved seismic performance. However, this observation is limited to the investigated steel ratios, ground-motion set,

and column geometry. Additional studies considering variations in axial load ratio, concrete strength, and higher seismic hazard levels are required before establishing generalized design recommendations.

- From a durability perspective, increasing the flange width, flange thickness, web height or web thickness improves seismic performance; however, excessive steel dimensions may reduce the effective concrete cover, which is critical for corrosion protection in cold regions subjected to de-icing salts. For bridge applications in severe Canadian winter environments, maintaining sufficient concrete cover while optimizing steel configuration is recommended to ensure a balanced design addressing both seismic performance and long-term durability.

Author Contributions: Conceptualization, M.M. and M.H.; methodology, M.M. and M.H.; writing—original draft preparation, M.M.; writing—review and editing, M.H.; supervision, M.H. All authors have read and agreed to the published version of the manuscript.

Funding: This research received funding from the Natural Sciences and Engineering Research Council of Canada (NSERC) through a Discovery Grant [Grant Number: CRSNG RGPIN-2024-04009].

Institutional Review Board Statement: Not applicable.

Informed Consent Statement: Not applicable.

Data Availability Statement: Data are available from the corresponding author upon reasonable request.

Conflicts of Interest: The authors declare no conflicts of interest.

References

1. American Institute of Steel Construction (AISC). *Load and Resistance Factor Design of W-Shapes Encased in Concrete*; American Institute of Steel Construction: Chicago, IL, USA, 2023.
2. Chen, C.C.; Lin, N.J. Analytical model for predicting axial capacity and behavior of concrete encased steel composite stub columns. *J. Constr. Steel Res.* **2006**, *62*, 424–433. [CrossRef]
3. Ellobody, E.; Young, B. Numerical simulation of concrete encased steel composite columns. *J. Constr. Steel Res.* **2011**, *67*, 211–222. [CrossRef]
4. El-Tawil, S.; Deierlein, G.G. Strength and Ductility of Concrete Encased Composite Columns. *J. Struct. Eng.* **1999**, *125*, 1009–1019. [CrossRef]
5. Campian, C.; Nagy, Z.; Pop, M. Behavior of Fully Encased Steel-Concrete Composite Columns Subjected to Monotonic and Cyclic Loading. *Procedia Eng.* **2015**, *117*, 439–451. [CrossRef]
6. Lai, B.; Richard Liew, J.Y.; Wang, T. Buckling behaviour of high strength concrete encased steel composite columns. *J. Constr. Steel Res.* **2019**, *154*, 27–42. [CrossRef]
7. Naito, H.; Akiyama, M.; Suzuki, M. Ductility Evaluation of Concrete-Encased Steel Bridge Piers Subjected to Lateral Cyclic Loading. *J. Bridg. Eng.* **2011**, *16*, 72–81. [CrossRef]
8. Mattock, A.H. Rotational capacity of hinging regions in reinforced concrete beams. *ACI* **1965**, *SP12*, 85–142.
9. Xu, C.; Cao, P.Z.; Wu, K.; Lin, S.Q.; Yang, D.G. Experimental investigation of the behavior composite steel-concrete composite beams containing different amounts of steel fibres and conventional reinforcement. *Construct. Build. Mater.* **2019**, *202*, 23–36. [CrossRef]
10. Chen, C.; Wang, C.; Sun, H. Experimental Study on Seismic Behavior of Full Encased Steel-Concrete Composite Columns. *J. Struct. Eng.* **2014**, *140*. [CrossRef]
11. Sheikh, S.A.; Uzumeri, S. Analytical model for concrete confinement in tied columns. *J. Struct.* **1982**, *108*, 2703–2722. [CrossRef]
12. Hassan, W.; Farag, M. Seismic performance of steel-reinforced concrete composite columns in existing and modern construction. *Soil Dyn. Earthq. Eng.* **2021**, *151*, 106945. [CrossRef]
13. Shang, C.; Xue, Y.; Yang, Y.; Yu, Y.; Yu, J. Lateral load–displacement response of flexure-dominant concrete-encased steel columns based on ASCE/SEI 41. *J. Constr. Steel Res.* **2023**, *203*, 107845. [CrossRef]
14. Idriss, L.K.; Gamal, Y.A.S. Predicting concrete-encased column behavior under uniaxial load using adaptive neural fuzzy systems. *Expert Syst. Appl.* **2025**, *278*, 127354. [CrossRef]

15. Wang, D.; Liu, Q.; Song, Y.; Zhu, Y.; Zhang, Y. Experimental and numerical study on seismic behaviors of SRC column–RC slab joints in NPP. *Nucl. Eng. Technol.* **2025**, *57*, 103176. [CrossRef]
16. Moradian, M.; Hassan, M. The Seismic Behavior of Rectangular Concrete-Encased Steel Bridge Piers: A Review. *Appl. Sci.* **2024**, *14*, 6627. [CrossRef]
17. *CAN/CSA S6-25*; Canadian Highway Bridge Design Code. Canadian Standards Association (CSA): Mississauga, ON, Canada, 2025.
18. Zhu, W.; Jia, J.; Gao, J.; Zhang, F. Experimental study on steel reinforced high-strength concrete columns under cyclic lateral force and constant axial load. *Eng. Struct.* **2016**, *125*, 191–204. [CrossRef]
19. CSI, Computer & Structures. *CSiBridge-Integrated Software for Structural Analysis and Design*; CSI, Computer & Structures: Berkeley, CA, USA, 2026.
20. *CAN/CSA A23.3-24*; Design of Concrete Structures. Canadian Standards Association (CSA): Mississauga, ON, Canada, 2024.
21. *CAN/CSA S16-24*; Design of Steel Structures. Canadian Standards Association (CSA): Mississauga, ON, Canada, 2024.
22. Hsu, H.-L.; Jan, F.-J.; Juang, J.-L. Performance of composite members subjected to axial load and bi-axial bending. *J. Constr. Steel Res.* **2009**, *65*, 869–878. [CrossRef]
23. Spacone, E.; Filippou, F.C.; Taucer, F.F. Fiber beam–column model for non-linear analysis of R/C frames: Part I. Formulation. *Earthq. Eng. Struct. Dyn.* **1996**, *25*, 711–725. [CrossRef]
24. Mander, J.B.; Priestley, M.J.; Park, R. Theoretical stress–strain model for confined concrete. *J. Struct. Eng.* **1988**, *114*, 1804–1826. [CrossRef]
25. Chen, S.; Wu, P. Analytical model for predicting axial compressive behavior of steel reinforced concrete column. *J. Constr. Steel Res.* **2016**, *128*, 649–660. [CrossRef]
26. *CSA Standard No. G30.18:21*; Carbon Steel Bars for Concrete Reinforcement. Canadian Standards Association: Toronto, ON Canada, 2021.
27. *CSA G40.20-13/G40.21-13*; General Requirements for Rolled or Welded Structural Quality Steel/Structural Quality Steel. Canadian Standards Association: Toronto, ON Canada, 2013.
28. Atkinson, G.M. Earthquake time histories compatible with the 2005 National building code of Canada uniform hazard spectrum. *Can. J. Civ. Eng.* **2009**, *36*, 991–1000. [CrossRef]
29. Tremblay, R.; Atkinson, G.M.; Bouaanani, N.; Daneshvar, P.; Léger, P.; Koboevic, S. Selection and scaling of ground motion time histories for seismic analysis using NBCC. In Proceedings of the 11th Canadian Conference on Earthquake Engineering (11CCEE), Victoria, BC, Canada, 23 July 2015.
30. Hancock, J.; Watson-Lamprey, J.; Abrahamson, N.A.; Bomer, J.J.; Markatis, A.; Mccoy, E.; Mendis, R. An improved method of matching response spectra of recorded earthquake ground motion using wavelets. *J. Earthq. Eng.* **2006**, *10*, 67–89. [CrossRef]
31. Lòpez, O.A.; Hernàndez, J.J.; Bonilla, R.; Fernàndez, A. Response spectra for multicomponent structural analysis. *Earthq. Spectra* **2006**, *22*, 85–113. [CrossRef]
32. Khaled, A.; Tremblay, R.; Massicotte, B. Combination rule for the prediction of the seismic demand on columns of regular bridges under bidirectional earthquake components. *Can. J. Civ. Eng.* **2011**, *38*, 698–709. [CrossRef]